journal

J. Am. Ceram. Soc., 1–7 (2016)
DOI: 10.1111/jace.14310

Conversion of Nuclear Waste to Molten Glass: Cold-Cap Reactions in Crucible Tests

Kai Xu,[‡,†] Pavel Hrma,[‡,†] Jarrett A. Rice,[‡] Michael J. Schweiger,[‡] Brian J. Riley,[‡] Nicole R. Overman,[‡] and Albert A. Kruger[§]

[‡]Pacific Northwest National Laboratory, Richland, Washington 99352

[§]U.S. Department of Energy, Office of River Protection, Richland, Washington 99352

The feed-to-glass conversion, which comprises complex chemical reactions and phase transitions, occurs in the cold cap during nuclear waste vitrification. To investigate the conversion process, we analyzed heat-treated samples of a simulated high-level waste feed using X-ray diffraction, electron probe microanalysis, leaching tests, and residual anion analysis. Feed dehydration, gas evolution, and borate phase formation occurred at temperatures below 700°C before the emerging glass-forming melt was completely connected. Above 700°C, intermediate aluminosilicate phases and quartz particles gradually dissolved in the continuous borosilicate melt, which expanded with transient foam. Knowledge of the chemistry and physics of feed-to-glass conversion will help us control the conversion path by changing the melter feed makeup to maximize the glass production rate.

Keywords: *nuclear waste; glass; reaction path*

I. Introduction

Approximately 200 000 m^3 of radioactive nuclear waste is currently stored at the Hanford Site. This waste is a byproduct of spent nuclear fuel reprocessing for plutonium production between 1944 and 1989.[1,2] The reprocessing was comprised of chemical dissolution of cladding and the fuel, as well as the extraction of plutonium from unwanted radionuclides and chemicals using various techniques, such as bismuth phosphate coprecipitation and the REDOX and PUREX processes.[2] The acidic wastes rendered alkaline were further processed to remove water, uranium, and desired radionuclides.[2,3] The resulting highly complex waste streams are stored in 177 carbon-steel underground tanks near Richland, Washington, USA. To reduce and manage the environmental risk, these wastes will be immobilized into the form of glass for long-term disposal.[4,5] The Hanford Tank Waste Treatment and Immobilization Plant (WTP), currently under construction, will separate the tank wastes into low-volume, high-level waste (HLW) (~95% of the waste radioactivity) and high-volume, low-activity waste (~90% of the waste mass) fractions to which glass-forming and -modifying chemicals will be added. The resulting melter feed will be converted to glass in joule-heated melters.[6–8]

Melter feed, a water-based mixture of waste and glass-forming and -modifying chemicals, typically contains more than 20 components. In the WTP, the melter feed will be charged from the top of waste-glass melters in the form of slurry. The feed-to-glass conversion occurs in the cold cap—a layer of reacting feed floating on the pool of molten glass.[9–12] As the feed moves down through the cold cap from the top, where the temperature can be as low as 100°C, to the bottom, where the temperature typically reaches to 1100°C, it is converted to molten glass through complex chemical reactions and phase transitions.[10–13] Feed-to-glass conversion usually consists of five stages: (i) evaporation and release of water, (ii) melting and decomposition of oxy-ionic salts, including mainly carbonates and nitrates/nitrites, (iii) formation of an early glass-forming (borate) melt and intermediate crystalline phases, (iv) dissolution of refractory particles, such as quartz and zirconia, and (v) expansion and collapse of foam.[14]

The reaction kinetics of feed-to-glass conversion was investigated using thermal analysis techniques including differential scanning calorimetry-thermogravimetric analysis (DSC-TGA) and gas chromatography-mass spectrometry (GC-MS).[15,16] Further information regarding feed reactions and phase transitions that cannot be identified with those techniques were investigated using laboratory-scale melter tests and crucible tests.[13,17,18] Detailed understanding of all stages of feed-to-glass conversion as they occur over the temperature range in the cold cap is needed for advanced melter feed formulation to enhance the glass production rate.[11,14]

In our previous study,[17] we reported about feed dehydration, gas evolution, and borate phase formation that occurred below 700°C, at which point the emerging melt was not completely connected and the gas-liberating reactions were virtually complete. Above this temperature, changes continue to occur within the continuous melt, which turns from borate into the final borosilicate glass-forming composition while intermediate crystalline phases form and dissolve, quartz particles dissolve, foam develops and collapses, and finally the melt homogenizes, approaching a compositionally uniform mixture.

This study covers feed-to-glass conversion over the entire cold-cap temperature span, from 100°C to 1100°C, focusing on the final stages. Crystalline phases were identified with X-ray diffraction (XRD). Elemental distribution, especially of boron, was mapped with wavelength dispersive X-ray spectroscopy (WDS). The fraction of soluble borate phase was determined by leaching the heat-treated samples in hot water and analyzing the leachate. Residual anions of carbonate, nitrate, and nitrite in heated samples were analyzed and compared with evolved gas analysis (EGA) data. Finally, we discuss the implications of the results for the nuclear waste vitrification in the WTP melter.

II. Experimental Procedure

(1) Feed Preparation and Heat Treatment

We used a melter feed for a simulated high-alumina HLW glass (Table I) that has been characterized in previous

E. Vance—contributing editor

Manuscript No. 38161. Received February 5, 2016; approved April 15, 2016.
[†]Authors to whom correspondence should be addressed. e-mails: kai.xu@pnnl.gov or pavel.hrma@pnnl.gov

studies.[13,15–20] The feed was prepared as slurry, as described in a previous paper.[20] Table I lists the batch chemicals used for slurry preparation and the target glass composition. The slurry was mixed and dried on a hot plate, and then heated at 105°C overnight in an oven. Silica was added as crushed quartz with a maximum particle size of 75 μm. Dry feed samples of approximately 10 g were heated in open Pt crucibles at the rate of 5 K/min to test temperatures (up to 1100°C), from which they were quenched in the air.

(2) Analyses of Heat-Treated Feed Samples

(A) X-Ray Diffraction: XRD analysis was conducted on the samples heated to temperatures between 100°C and 1200°C in 100°C intervals with a Bruker® D8 Advance diffractometer (Bruker AXS Inc., Madison, WI) equipped with CuK_α emission (λ = 1.5406 Å) at a power of 40 kV and 40 mA. Heat-treated samples were mixed with 5 mass% of a CaF_2 standard for quantitative analysis. The powdered samples were scanned from 5° to 80° 2θ with a step size of 0.015° 2θ and a 1.5 s dwell at each step. Crystalline phases from the XRD patterns were identified with Bruker AXS DIFFRAC^{plus} EVA software and the mass fractions of crystalline phases were quantified with TOPAS 4.2 software (Bruker AXS Inc., Madison, WI).

(B) Electron Probe Microanalysis–Wavelength Dispersive X-Ray Spectroscopy: Four representative samples (heated up to 400°C, 600°C, 800°C, and 1000°C) were analyzed using an electron probe microanalyzer (EPMA; JXA-8530F HyperProbe; JEOL USA Inc., Peabody, MA) with a field-emission gun and five wavelength dispersive X-ray spectrometers. Backscattered electron microscopy and compositional mapping of B, Na, Al, Ca, and Fe were performed to evaluate structural change in feed and elemental distribution as the function of heating. Measurement was accomplished using an accelerating voltage of 20 kV, a probe current of 9.9×10^{-8} A, dwell time of 100 ms and a step spacing of 0.2 μm. An LDE2 crystal was used for mapping boron. Samples were cast or mounted in an epoxy resin, and polished in an oil-based diamond suspension to prevent dissolution of water-soluble species before analysis.

(C) Leaching Test: Leaching tests were performed on heat-treated samples to observe the evolution of borate phase. Samples heated below 700°C remained in the form of powder and were lightly crushed using an agate mortar and pestle to pulverize larger clumps. Samples heated above 700°C formed a hard mass that was ground and sieved through a 200-mesh (~74 μm) sieve. A 5-g powdered sample was added to 100 mL deionized water in a 300-mL closed Teflon vessel. The vessel was then kept in an oven at 80°C for 24 h. Afterward, an aliquot of 5 mL solution was filtered through a 0.45-μm filter using a 10-mL syringe with for elemental analysis. Inductively coupled plasma atomic emission spectroscopy (ICP-AES) was performed by Southwest Research Institute (SwRI, San Antonio, TX).

(D) Residual Anion Analysis: Samples heated from 100°C to 650°C at 50°C intervals were sent to SwRI for anion analysis. Total inorganic carbon was determined using a Dohrmann DC 80 analyzer (Dohrmann Instruments Company, Santa Clara, CA). Nitrate and nitrite were extracted with deionized water, and the extract was analyzed by ion chromatography.

(E) Data Processing: Since melter feed gradually loses mass as gases are released with increasing temperature, the content of crystalline phases is expressed as mass fractions related to the final glass.[17]

The fraction of the i^{th} element dissolved was calculated using the formula $d_i = Vc_i/m_g g_i$, where V is the solution volume (100 mL), c_i is the i^{th} element concentration analyzed from ICP-AES (mass per volume), g_i is the i^{th} element mass

Table I. Batch Composition (g) to Make 1 kg of Glass and Target Glass Composition

Batch composition	g/kg	Glass composition	Mass%	Mol.%
SiO_2	305.05	SiO_2	30.50	35.05
$Al(OH)_3$	367.49	Al_2O_3	24.00	16.25
H_3BO_3	269.83	B_2O_3	15.21	15.09
Li_2CO_3	88.30	Li_2O	3.57	8.25
CaO	60.79	CaO	6.09	7.50
$Fe(OH)_3$	73.82	Fe_2O_3	5.91	2.56
$Fe(H_2PO_2)_3$	12.42	Na_2O	9.59	10.68
NaOH	99.41	K_2O	0.14	0.10
NaF	14.78	MgO	0.12	0.21
Na_2CrO_4	11.13	ZrO_2	0.39	0.22
Na_2SO_4	3.55	ZnO	0.08	0.07
$NaNO_2$	3.37	Bi_2O_3	1.14	0.17
$Na_2C_2O_4$	1.26	NiO	0.40	0.37
KNO_3	3.04	PbO	0.41	0.13
$Mg(OH)_2$	1.69	Cr_2O_3	0.52	0.24
$Zr(OH)_4{\cdot}0.65H_2O$	5.49	P_2O_5	1.05	0.51
$Zn(NO_3)_2{\cdot}4H_2O$	2.67	SO_3	0.20	0.17
$Bi(OH)_3$	12.80	F	0.67	2.44
$NiCO_3$	6.36			
$Pb(NO_3)_2$	6.08			
Total	1349.33	Total	100.00	100.00

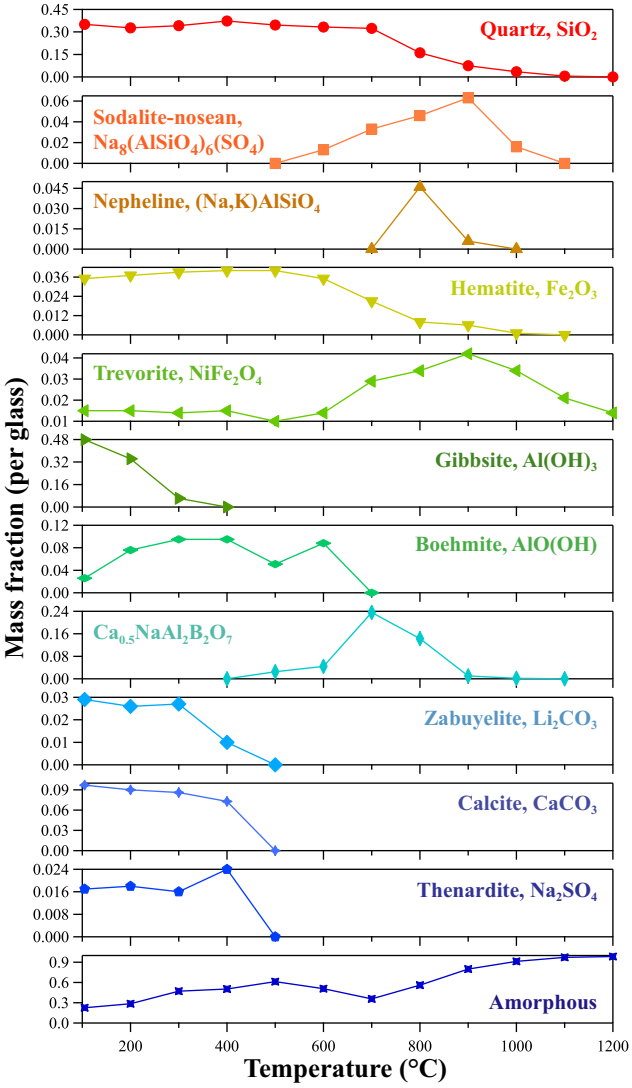

Fig. 1. Mass fraction of each phase in the feed with respect to glass versus heat-treatment temperature.

fraction in glass, and m_g is the final glass mass. The final glass mass was determined as $m_g = m_f(1-L)/(1-L_G)$, where m_f is the heat-treated sample mass (5 g), L is the mass-loss fraction of the dry feed heated to each test temperature, and L_G is the mass-loss fraction of the dry feed heated to 1100°C, at which point the sample converted to molten glass. The measured value of L_G was ~0.21. This value is different from the fraction of volatile constituents (~0.25) in the as-batched feed (Table I) because of the loss of bonded water and the uptake of CO_2 from the air during slurry preparation and subsequent drying.

The content of gases (CO_2 and NO, as identified with GC-MS[16]) determined by anion analysis was expressed as the mass of gases remaining in the initial dry feed, $\Gamma_i = \gamma_i(1-L)$, where γ_i is the i^{th} gas remaining in the heat-treated samples; $i \equiv CO_2$ and NO.

III. Results

(1) XRD

Figure 1 displays the fraction of each phase in the feed with respect to glass as functions of heat-treatment temperature. In agreement with previous works,[21,22] the fraction of quartz (SiO_2) remained constant until 500°C, then started to decrease, and dropped to almost zero at 1100°C. Sodalite [$Na_8(AlSiO_4)_6(SO_4)$] and nepheline [$(Na,K)AlSiO_4$] appeared at 600°C and 800°C, respectively, reached their maximum fractions at ~900°C and ~800°C, respectively, and finally were gone above ~1000°C. Interestingly, hematite (Fe_2O_3) and trevorite ($NiFe_2O_4$) had already formed in the initial dry feed. While hematite was present at an almost constant level until 500°C and disappeared by 1000°C, a small content of trevorite remained in the samples throughout the cold-cap temperature range; its maximum fraction occurred at 900°C when hematite was gone. Similar to the previous study,[17] gibbsite [$Al(OH)_3$] remained stable during feed preparation and dehydrated as temperature increased to 300°C, turning into amorphous alumina and boehmite (AlOOH). As temperature increased further to 500°C, an intermediate borate phase ($Ca_{0.5}NaAl_2B_2O_7$) appeared, reached its maximum level at 700°C, consuming boehmite and amorphous alumina, and finally disappeared by 1000°C. Salt phases, including carbonates and sulfates, remained in the dry feed and disappeared by 500°C. The fraction of amorphous phase (or, more precisely, phases unidentified as crystalline, including a sodium borate phase formed during feed preparation) increased with dehydration of gibbsite, decreased with the emergence of the intermediate borate phase at 700°C, and finally reached ~100% at 1100°C.

(2) EPMA-WDS

Samples heated below 700°C were comprised of loose grains of feed, whereas the sample volume shrank and became a firm mass when temperature increased to 800°C. Figure 2 shows backscattered electron images of samples heated to 800°C and 1000°C. At 800°C, the connected body of glass-forming melt [Fig. 2(a)] encapsulates various crystalline phases [light gray areas in Fig. 2(b)]. Note that undissolved quartz particles, indicated by arrows, retained their sharp edges [Fig. 2(b)], and small irregularly shaped voids [black areas in Fig. 2(a)] are observed throughout the sample. Between 800°C and 1000°C, gas bubbles of ~100 to ~1000 μm in diameter turned the reacting feed into foam [Fig. 2(c)], causing the sample to expand, whereas small crystals of trevorite remained and dissolving quartz particles became rounder [Fig. 2(d)]. The bubbles escaped by 1100°C when the feed was converted to glass.

To identify the boron phases, feed samples heated to 400°C, 600°C, 800°C, and 1000°C were analyzed with WDS (Fig. 3). At 400°C, most B (in white boxes) appeared together with Na, indicating the formation of sodium borate, whereas Al and Ca were predominantly accumulated as inclusions. At 600°C, B showed less correlation with Na, and started to associate with Al and Ca. As temperature increased to 800°C, B mainly occurred with Na, Al and Ca, possibly because of the formation of borate phases, such as $Ca_{0.5}NaAl_2B_2O_7$. At 1000°C, B and Na formed continuous melt in which they were almost uniformly dispersed, whereas only trevorite crystals and quartz residues remained.

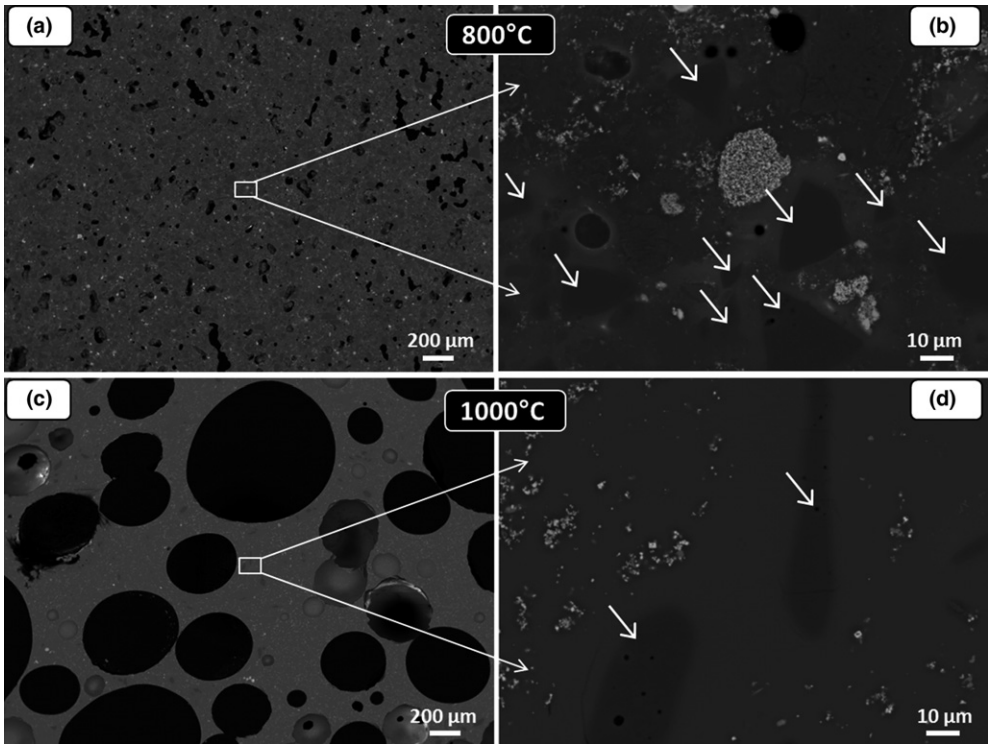

Fig. 2. Backscattered electron micrographs of feed samples heated to (a, b) 800°C and (c, d) 1000°C. Arrows in Figs. 2(b) and (d) indicate quartz particles. In Fig. 2(d), bright spots are crystals of trevorite ($NiFe_2O_4$).

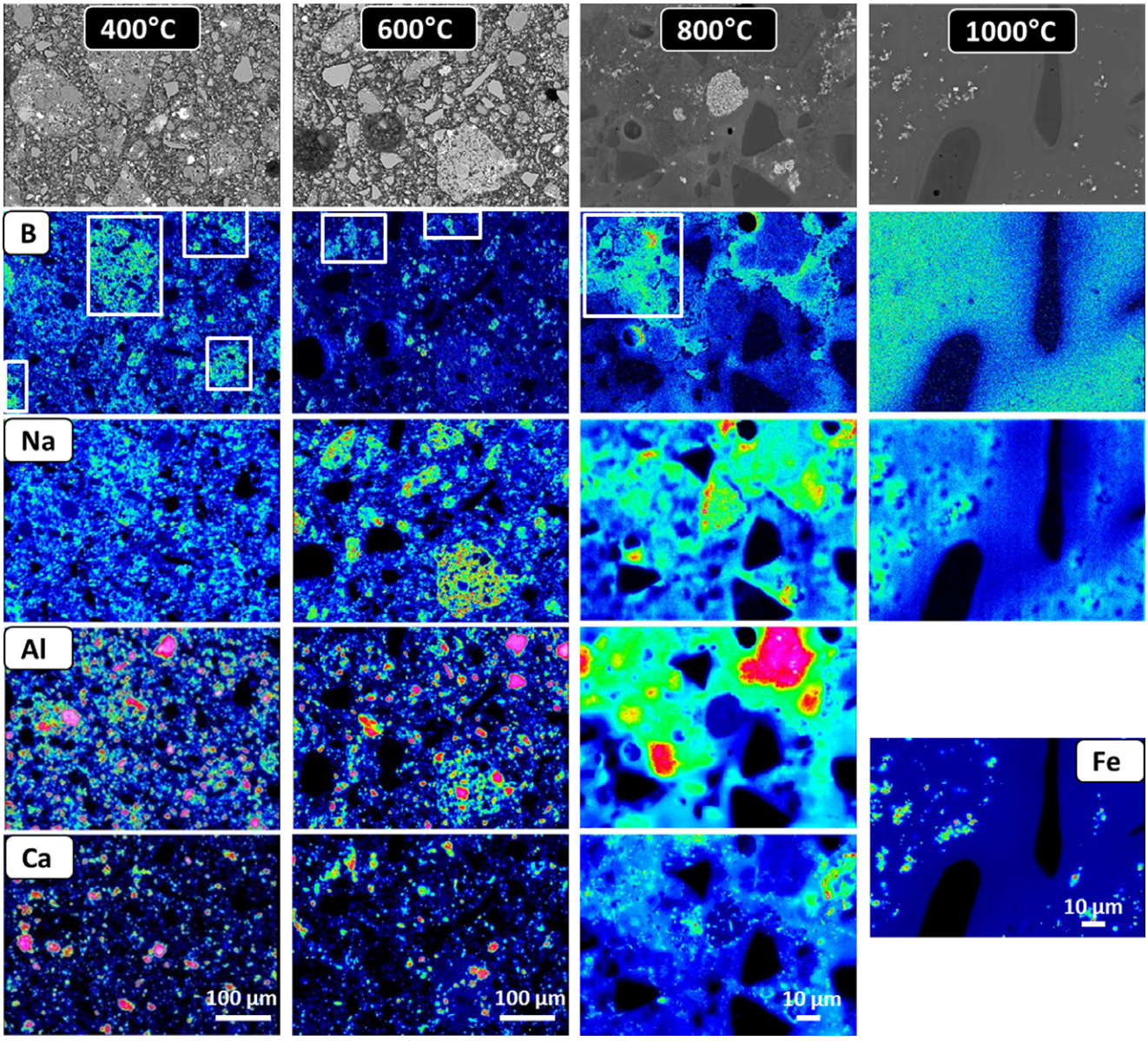

Fig. 3. Elemental maps of feed samples heated to 400°C, 600°C, 800°C, and 1000°C. Rainbow scaling is used to show concentration gradients in the elemental maps (red color indicates the highest concentration). The Fe map of the sample heated to 1000°C shows the presence of trevorite crystals [bright spots in Fig. 2(d)].

(3) Leaching Tests

Development of borate phases can be traced from the fractions of key elements (B, Na, Li, Al, Ca, and Si) dissolved from the heat-treated samples in hot water. As Fig. 4(a) shows, the dissolved fractions of B and Na are close; almost all B and Na dissolved from samples heated below 400°C. The dissolved fractions continued to decrease as temperature increased above 500°C and finally dropped to zero at 900°C. Because Li_2CO_3 has a low water solubility,[23] the dissolved fraction of Li was lower than that of B or Na [Fig. 4(a)]. The Al and Ca started to dissolve at 400°C, reached maximum at ~700°C, and eventually became components of hot-water insoluble phases at ~1000°C [Fig. 4(b)]. Above 700°C, tiny fractions of dissolved Si were detected that gradually increased with the heat-treatment temperature [Fig. 4(c)]. Because of the experimental uncertainty, the leaching test provides only approximate dissolved fractions, but shows the dissolution trends of those elements as functions of heat-treatment temperature.

(4) Residual Anion Analysis

Figure 5(a) plots CO_2 and NO content (Γ_i) versus temperature. The residual carbonates and nitrates/nitrites remained at almost constant levels until 400°C, when they started to decrease, and were virtually gone by 700°C. Figure 5(b) shows the gas evolution rate ($d\Gamma_i/dT$). Both CO_2 and NO peaked at ~500°C, the CO_2 evolution peak being wider. The content of CO_2 and NO in the initial dry feed calculated from the batch composition in Table I is also included in Fig. 5(a). The measured content of CO_2 (~0.06 g/g) is larger than the batched content (~0.04 g/g), indicating extra CO_2 taken up from the atmosphere. This CO_2 probably reacted with CaO to form $CaCO_3$, which was detected with XRD. The measured and batched NO were almost identical.

IV. Discussion

(1) Cold-Cap Reactions at 100°C ≤ T ≤ 700°C

As reported in our previous paper,[17] cold-cap reactions below 700°C comprise dehydration of feed (T < 400°C), evolution of CO_2 and NO (400°C ≤ T ≤ 700°C), and formation of borate phases. In this work, we traced the transformation of borate phases with WDS and leaching tests. No crystalline sodium borates that formed when NaOH reacted with H_3BO_3 in the slurry were identified with XRD. However, the elemental mapping of the sample heat-treated to 400°C

(Fig. 3) showed that most Na was associated with B in unidentified, most likely amorphous, sodium borate phases. We estimated the composition (in terms of component mass fractions) of the amorphous phase based on the batch composition and chemical composition of crystalline phases identified with XRD (Fig. 6), according to which sodium borates contributed ~75% to the amorphous phases in the dry feed.

The proportion in which B and Na dissolved in hot-water leaching changed little with temperature [Fig. 4(a)]. The extra Na that dissolved at temperatures below 600°C [Fig. 4(a)] came from water-soluble salts, that is, $NaNO_2$, NaF, Na_2SO_4, and Na_2CrO_4 (Table I). Releases of Al and Ca were detected starting at 400°C [Fig. 4(b)], indicating that amorphous alumina from dehydration of gibbsite and calcium oxides from decomposition of calcite (Fig. 6) were gradually incorporated into the borate phase. This intermediate phase $Ca_{0.5}NaAl_2B_2O_7$, identified with XRD, resulted in the increasingly durable borate phase [Fig. 4(a)], but less durable aluminate phase [Fig. 4(b)]. Below 700°C, the amorphous borate phase formed disconnected pockets of melt.

The gases, CO_2 and NO, began to evolve at ~300°C and ~400°C, respectively. Their evolution peaked at ~500°C (Fig. 5), ~100°C higher than from the EGA analysis.[16] This discrepancy was probably caused by the temperature gradient in the large crucible sample[24,25] and by the low partial pressure of the evolving gases due to the diffusion of the carrier gas into the tiny EGA sample. Similar to the EGA analysis, the gas-liberating reactions virtually ceased around 700°C [Fig. 5(a)].

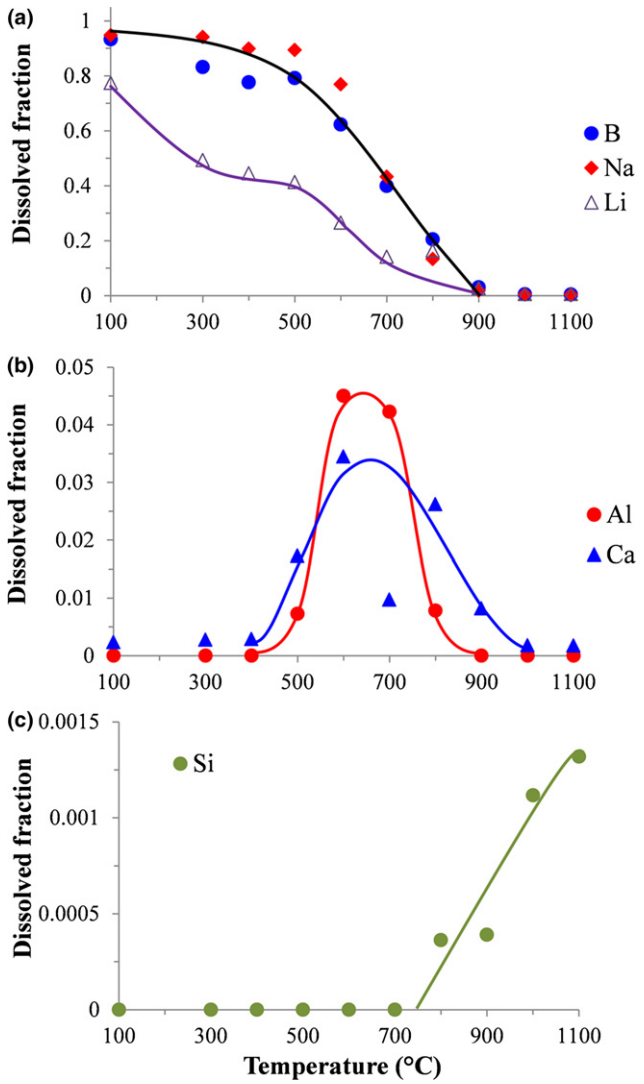

Fig. 4. Fractions of (a) B, Na, and Li, (b) Al and Ca, and (c) Si dissolved during 24 h from heat-treated samples leached in hot (80°C) water as functions of heat-treatment temperature. Lines were added as guides for the eyes.

(2) Cold-Cap Reactions at 700°C < T ≤ 1100°C

Above 700°C, cold-cap reactions involved the emergence of a borosilicate melt associated with dissolution of quartz, formation of intermediate aluminosilicate phases, and expansion and collapse of foam. The released fractions of Al and Ca reached their maximum levels at ~700°C and then decreased

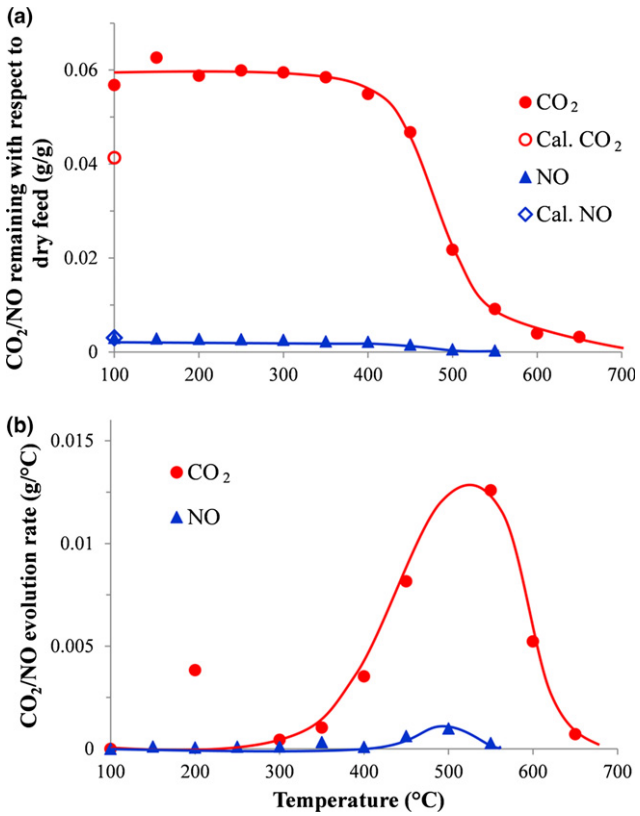

Fig. 5. (a) Mass (g) of CO_2 and NO remaining with respect to dry feed (g) as functions of heat-treatment temperature (○ and ◊ denote masses of CO_2 and NO, respectively, in initial dry feed calculated from the batch composition listed in Table I). (b) CO_2 and NO evolution rate (g/°C) with temperature. Lines were added as guides for the eyes.

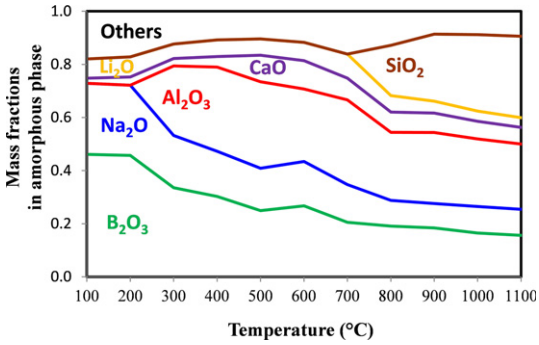

Fig. 6. Amorphous phase composition versus heat-treatment temperature. Mass fractions were assessed based on the initial batch composition and chemical composition of crystalline phases identified with XRD. The component "Others" includes Fe_2O_3 and the rest of the minor components, such as PbO, Cr_2O_3, ZrO_2, etc.

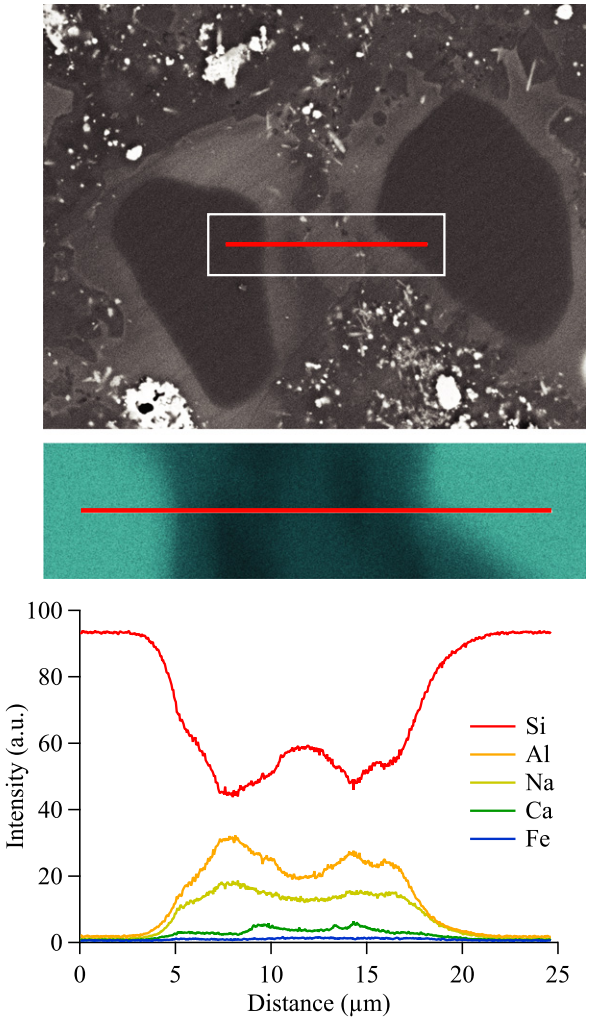

Fig. 7. (Top) Backscattered electron micrograph showing two adjacent dissolving quartz particles in the sample heated to 800°C, (middle) Si elemental map (higher concentration in darker blue), (bottom) a line scan at the line defined in the above images. Scanning electron microscopy (SEM) (JSM-7001F; JEOL USA, Inc. Peabody, MA) was used for looking at morphology of the silica grains in the sample using a different instrument than the EPMA. This SEM was equipped with an EDAX Si-drift energy-dispersive X-ray spectrometer (EDS) (Apollo XL; AMETEK, Berwyn, PA) for elemental dot mapping and postmap line scan analysis.

[Fig. 4(b)], as the content of SiO_2 increased in the amorphous phase (Fig. 6) and Si started to release in hot water [Fig. 4(c)]. While the intermediate silicate phases, such as sodalite and nepheline (Fig. 1) formed and then dissolved in the glass-forming melt, and the melt was increasingly homogeneous [Figs. 2(d) and 3], dissolving quartz particles were surrounded by concentration layers of high silica content.[20] Figure 7 shows Si elemental map of the sample heated to 800°C. Note the enhanced concentration of Si between (and around) quartz particles (the line scan in Fig. 7).

The feed expansion test[14,26] showed that the feed volume shrank starting at 700°C and reached a minimum at ~800°C when the glass-forming melt became fully connected. As the temperature increased above 800°C, the melt began to expand, creating foam. Bubbles from residual gases can be seen in Fig. 2(c). As the temperature increased, the viscosity of glass-forming melt decreased[27] and bubbles grew and coalesced, leading to collapse of foam.

(3) Implications for WTP Nuclear Waste Melter

Thermoanalytical methods (TGA and DSC) determine the kinetics of feed conversion reactions, but cannot identify their nature.[15,28] The methods used in this work—XRD, EPMA-WDS, leaching, and residual anion analysis, together with the EGA[16] and the feed expansion test[14,26,29]—allow us to gain still limited, yet substantial, insight into the chemistry and physics of feed conversion reactions and their transitory products. Thus, we gain knowledge about the crystalline, amorphous, and gaseous phases as they evolve in response to heating at a rate representative of the temperature history that the melter feed experiences when turning into molten glass within the cold cap.

The key issue for the performance of WTP HLW melters is achieving a steady undisturbed process that proceeds at a high rate of conversion. The performance criteria are affected by the temperature at which the glass-forming melt connects, the evolution and collapse of foam, the rate and extent of formation and dissolution of solid phases, and various other phenomena that can be controlled, or at least influenced, by the melter feed makeup, that is, the physical and chemical form of the glass-forming and -modifying additives.

The lower layer of the cold cap, where the connected glass-forming melt has a tendency to become foam, limits the heat flux to the upper layer, where most of the heat is consumed by water evaporation, feed reactions, and the formation or dissolution of phases. The extent of foaming can be

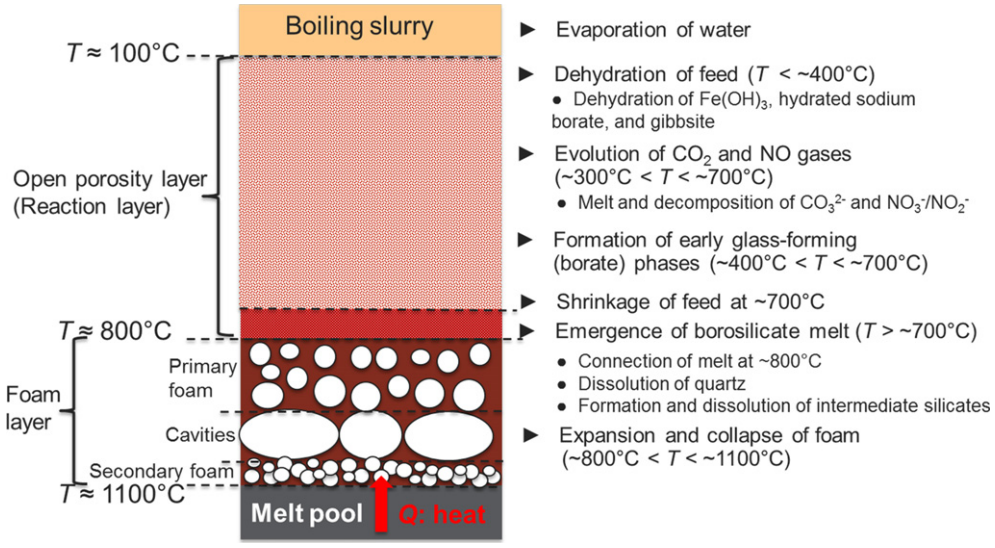

Fig. 8. Schematic diagram of feed-to-glass conversion in the cold cap.

reduced by manipulating the evolution of crystalline, amorphous, and residual gaseous phases.

Briefly, melter feed makeup affects the rate of feed-to-glass conversion, and thus the rate of melting, in both the upper and lower layers of the cold cap. Understanding this process is thus vital for the HLW vitrification performance. The glass production rate directly influences the life cycle of nuclear waste cleanup. The cleanup time can be shortened by 50% if either the capacity of the vitrification plant doubles or the rate of melting doubles. Each of these options substantially reduces the risk to the environment, but the latter option is far less expensive.

V. Summary

Cold-cap reactions of a melter feed for vitrifying a high-alumina HLW were investigated with XRD, EMPA-WDS, leaching tests, and residual anion analysis. The feed-to-glass conversion in the cold cap can be summarized as follows (see Fig. 8).

1. At 100°C $\leq T \leq$ 700°C, cold-cap reactions mainly consist of feed dehydration, gas evolution, and borate phase formation. The evolution of CO_2 and NO peaks at $\sim$500°C, and ceases around 700°C. Amorphous, or unidentified, sodium borate phases form during feed preparation and subsequently dehydrate, melt, and/or form intermediate borate phases as the temperature increases to 700°C.
2. At 700°C $< T \leq$ 1100°C, the early glass-forming melt turns to borosilicate as quartz grains dissolve. The intermediate silicate phases form and then dissolve. As the melt connects above 800°C, it begins to expand and creates foam. Above $\sim$1000°C, few solids remain, and foam starts to collapse into bubble-free molten glass.

Acknowledgments

This work was undertaken with funding authorized by the Federal Project Director William F. Hamel, Jr. of the U.S. Department of Energy (DOE), Waste Treatment and Immobilization Plant. Pacific Northwest National Laboratory is operated by Battelle Memorial Institute for the DOE under contract DE-AC05-76RL01830. The authors thank Jarrod Crum for quantitative XRD analysis, Clyde Chamberlin for polishing specimens, and Jaehun Chun, Derek Dixon, Seungmin Lee, and Steven A. Luksic for insightful discussions.

References

[1]M. S. Gerber, "History of Hanford Site Defense Production (Brief)"; HNF-5041-FP Rev. 0, Fluor Hanford, Richland, Washington, 2001.

[2]U.S. Department of Energy, Plutonium: The First 50 Years: United States Plutonium Production, Acquisition, and Utilization from 1944 Through 1994, DOE/DP-0137, Washington, DC, 1996.

[3]R. E. Gephart, "A Short History of Hanford Waste Generation, Storage, and Release"; PNNL-13605 Rev. 4, Pacific Northwest National Laboratory, Richland, Washington, 2003.

[4]R. H. Gray and C. D. Becker, "Environmental Cleanup: The Challenge at the Hanford Site, Washington, USA," *Environ. Manage.*, **17** [4] 461–75 (1993).

[5]K. D. Crowley and J. F. Ahearne, "Managing the Environmental Legacy of U.S. Nuclear-Weapons Production," *Am. Sci.*, **90**, 514–23 (2002).

[6]P. J. Certa, P. A. Empey, and M. N. Wells, "River Protection Project System Plan: Retrieve and Treat Hanford's Tank Waste and Close the Tank Farms to Protect the Columbia River"; ORP-11242 Rev. 6, Office of River Protection, U.S. Department of Energy, Richland, Washington, 2011.

[7]J. D. Vienna, "Nuclear Waste Vitrification in the United States: Recent Developments and Future Options," *Int. J. Appl. Glass Sci.*, **1** [3] 309–21 (2010).

[8]I. L. Pegg, "Turning Nuclear Waste into Glass," *Phys. Today*, **68** [2] 33–9 (2015).

[9]R. E. Eibling and C. A. Nash, "Hanford Waste Simulants Created to Support the Research and Development on the River Protection Project–Waste Treatment Plant"; WSRC-TR-2000-00338, Westinghouse Savannah River Company, Aiken, South Carolina, 2001.

[10]P. Hrma, A. A. Kruger, and R. Pokorný, "Nuclear Waste Vitrification Efficiency: Cold Cap Reactions," *J. Non-Cryst. Solids*, **358**, 3559–62 (2012).

[11]R. Pokorný and P. Hrma, "Mathematical Modeling of Cold Cap," *J. Nucl. Mater.*, **429**, 245–56 (2012).

[12]R. Pokorný, A. A. Kruger, and P. Hrma, "Mathematical Modeling of Cold Cap: Effect of Bubbling on Melting Rate," *Ceram.–Silikáty*, **58** [4] 296–302 (2014).

[13]D. R. Dixon, M. J. Schweiger, B. J. Riley, R. Pokorný, and P. Hrma, "Temperature Distribution Within a Cold Cap During Nuclear Waste Vitrification," *Environ. Sci. Technol.*, **49** [14] 8856–63 (2015).

[14]P. Hrma, M. Schweiger, C. Humrickhouse, J. Moody, R. Tate, et al., "Effect of Glass-Batch Makeup on the Melting Process," *Ceram.-Silikáty*, **54** [3] 192–211 (2010).

[15]J. Chun, D. A. Pierce, R. Pokorný, and P. Hrma, "Cold-Cap Reactions in Vitrification of Nuclear Waste Glass: Experiments and Modeling," *Thermochim. Acta*, **559**, 32–9 (2013).

[16]C. Rodriguez, J. Chun, M. J. Schweiger, A. A. Kruger, and P. Hrma, "Application of Evolved Gas Analysis to Cold-Cap Reactions of Melter Feeds for Nuclear Waste Vitrification," *Thermochim. Acta*, **592**, 86–92 (2014).

[17]K. Xu, P. Hrma, J. Rice, B. J. Riley, M. J. Schweiger, and J. V. Crum, "Melt Feed Reactions at $T \leq$ 700°C for Nuclear Waste Vitrification," *J. Am. Ceram. Soc.*, **98** [10] 3105–11 (2015).

[18]D. A. Pierce, P. Hrma, J. Marcial, B. J. Riley, and M. J. Schweiger, "Effect of Alumina Source on the Rate of Melting Demonstrated with Nuclear Waste Glass Batch," *Int. J. Appl. Glass Sci.*, **3** [1] 59–68 (2012).

[19]K. S. Matlack, H. Gan, M. Chaudhuri, W. Kot, W. Gong, et al., "Melt Rate Enhancement for High Aluminum HLW Glass Formulations"; VSL-08R1360-1, Vitreous State Laboratory, The Catholic University of America, Washington, DC, 2008.

[20]M. J. Schweiger, P. Hrma, C. J. Humrickhouse, J. Marcial, B. J. Riley, and N. E. TeGrotenhuis, "Cluster Formation of Silica Particles in Glass Batches During Melting," *J. Non-Cryst. Solids*, **356**, 1359–67 (2010).

[21]P. Hrma, J. Marcial, K. J. Swearingen, S. H. Henager, M. J. Schweiger, and N. E. TeGrotenhuis, "Conversion of Batch to Molten Glass, II: Dissolution of Quartz Particles," *J. Non-Cryst. Solids*, **357**, 820–8 (2011).

[22]R. Pokorný, J. A. Rice, J. V. Crum, M. J. Schweiger, and P. Hrma, "Kinetic Model for Quartz and Spinel Dissolution During Melting of High-Level-Waste Glass Batch," *J. Nucl. Mater.*, **443**, 230–5 (2013).

[23]W. M. Haynes, *CRC Handbook of Chemistry and Physics*, 92nd edition, pp. 5-190–5-195. CRC Press, Boca Raton, FL, 2011.

[24]R. Pokorný, J. A. Rice, M. J. Schweiger, and P. Hrma, "Determination of Temperature-Dependent Heat Conductivity and Thermal Diffusivity of Waste Glass Melter Feed," *J. Am. Ceram. Soc.*, **96** [6] 1891–8 (2013).

[25]J. A. Rice, R. Pokorný, M. J. Schweiger, and P. Hrma, "Determination of Heat Conductivity and Thermal Diffusivity of Waste Glass Melter Feed: Extension to High Temperatures," *J. Am. Ceram. Soc.*, **97** [6] 1952–8 (2014).

[26]K. Xu, D. A. Pierce, P. Hrma, M. J. Schweiger, and A. A. Kruger, "Rhenium Volatilization in Waste Glasses," *J. Nucl. Mater.*, **464**, 382–8 (2015).

[27]J. Marcial, J. Chun, P. Hrma, and M. J. Schweiger, "Effect of Bubbles and Silica Dissolution on Melter Feed Rheology During Conversion to Glass," *Environ. Sci. Technol.*, **48** [20] 12173–80 (2014).

[28]R. Pokorný, D. A. Pierce, and P. Hrma, "Melting of Glass Batch: Model for Multiple Overlapping Gas-Evolving Reactions," *Thermochim. Acta*, **541**, 8–14 (2012).

[29]Z. Hilliard and P. Hrma, "A Method for Determining Bulk Density, Material Density, and Porosity of Melter Feed During Nuclear Waste Vitrification," *J. Am. Ceram. Soc.*, **99** [1] 98–105 (2016). □